Journal of Groundwater Science and Engineering 14(2026) 32–48

Journal homepage: http://gwse.iheg.org.cn

Research Article

Application of the DITAPH model coupling human activities and groundwater dynamics for nitrate vulnerability assessment: A case study in Quanzhou, China

Jian-feng Li[1,2], Yuan-jing Zhang[1,2], Ya-ci Liu[1,2], Qi-chen Hao[1,2], Chun-lei Liu[1,2], Sheng-wei Cao[1,2], Zheng-hong Li[1,2*]

[1] *Fujian Provincial Key Laboratory of Water Cycling and Eco-Geological Processes*, *Xiamen* 361000, *Fujian Province*, *China*.
[2] *Institute of Hydrogeology and Environmental Geology*, *CAGS*, *Shijiazhuang* 050061, *China*.

Abstract: To address the deficiencies in comprehensive surface contamination prevention strategies within China's nitrate-affected regions, this research innovatively proposes the DITAPH model - a systematic framework integrating groundwater nitrate vulnerability assessment and Nitrate Vulnerable Zones (NVZs) delineation through optimization of hydrogeological parameters. Based on detailed hydrogeological and hydrochemical investigations, the DITAPH model was applied in the plain areas of Quanzhou to evaluate its applicability. The model selected hydrogeological parameters (depth of groundwater, lithology of the vadose zone, topographic slope, aquifer water yield property), one climatic parameter (precipitation), and two anthropogenic parameters (land use type and population density) as assessment indicators. The results of the groundwater nitrate vulnerability assessment showed that the low, relatively low, relatively high, and high groundwater nitrate vulnerability zones in the study area accounted for 5.96%, 35.44%, 53.74% and 4.86% of the total area, respectively. Groundwater nitrate vulnerability was most strongly influenced by human activities, followed by groundwater depth and topographic slope. The high vulnerability zone is mainly affected by domestic and industrial wastewater, whereas the relatively high groundwater nitrate vulnerability zone is primarily influenced by agricultural activities. Validation of the DITAPH model revealed a significant positive correlation between the DITAPH index (DI) and nitrate concentration ($\rho(NO_3^-)$). The results of the NVZs delineated by the DITAPH model are reliable and can serve as a tool for water resource management planning, guiding the development of targeted measures in the NVZs to prevent groundwater contamination.

Keywords: Nitrate contamination; NVZs delineation; Human activity coupling; Pollution risk management

Received: 27 Apr 2025/ Accepted: 09 Oct 2025/ Published: 18 Nov 2025

Introduction

Although approximately 66% of the global population (around 4 billion people) already faces periodic severe water scarcity (Mekonnen and Hoekstra, 2016), the ongoing deterioration of water quality-induced water scarcity—such as groundwater nitrate contamination—has further intensified the water resource crisis, posing a critical constraint on sustainable development.

As one of the most prevalent contaminants in groundwater (Abascal et al. 2022), nitrate exceeding safe levels in regions spanning Africa, Asia, and Europe has drawn widespread attention (Gutiérrez et al. 2018). Epidemiological studies confirm that chronic exposure to elevated nitrate concentrations is strongly associated with various cancers and infant methemoglobinemia (Chilaule et al. 2023), while also triggering eutrophication in

*Corresponding author: Zheng-hong Li, *E-mail address*: lizhenghong@mail.cgs.gov.cn

DOI: 10.26599/JGSE.2026.9280069

Li JF, Zhang YJ, Liu YC, et al. 2026. Application of the DITAPH model coupling human activities and groundwater dynamics for nitrate vulnerability assessment: A case study in Quanzhou, China. Journal of Groundwater Science and Engineering, 14(1): 32-48.

coastal ecosystems (Verma et al. 2023). To address this threat, the European Union established the Nitrate Vulnerable Zones (NVZs) framework through the Nitrates Directive (91/676/EEC), providing a global policy blueprint for groundwater management (Monteny, 2001).

The issue of groundwater nitrate contamination in China has become increasingly severe (Sun et al. 2023). Multi-regional studies have demonstrated that groundwater nitrate pollution caused by intensive agriculture and rapid urbanization has emerged as a widespread phenomenon (Kong et al. 2022). Scholars have reviewed methods for pollution source identification and remediation technologies for groundwater (Liu et al. 2024). However, China currently lacks a systematic vulnerability assessment framework that integrates hydrogeological characteristics with anthropogenic influences, along with risk assessment-based differentiated nutrient management strategies (Ma et al. 2018). This highlights an urgent need to develop regionally adaptable scientific assessment tools.

Among existing assessment methods, the DRASTIC model has become the most widely applied groundwater vulnerability evaluation framework due to its systematicity and operational feasibility (Khosravi et al. 2018). However, extensive empirical studies have revealed its inherent limitations:

(1) Redundancy in the parameter system, particularly the functional overlap between aquifer media and hydraulic conductivity coefficients (Martínez-Bastida et al. 2010);

(2) Challenges in accurately quantifying critical parameters (e.g., net recharge rate) due to complex surface processes (Chakraborty et al. 2022; Lubianetzky et al. 2015; Nahin et al. 2020; Yankey et al. 2021);

(3) Subjective weight assignments lacking objective justification (Hamza et al. 2015);

(4) Insufficient integration of anthropogenic influences (Stigter et al. 2006).

Although recent advancements have introduced improved approaches such as DRASTIC-AHP (Smail and Dişli, 2023) and machine learning techniques (Fu and Le, 2025; Zhao et al. 2025), inadequate precision in NVZ delineation remains a critical constraint on effective pollution control (Arauzo et al. 2022; Arauzo and Martínez-Bastida, 2015; Orellana-Macías et al. 2020).

To address these issues, this study proposes the innovative DITAPH model, with technical breakthroughs manifested in:

(1) A streamlined parameter system retaining core elements including Depth of groundwater (D), Lithology of the vadose zone (I), and Topographic slope (T), while incorporating Aquifer thickness (A) and Precipitation (P) to enhance hydrological process characterization;

(2) pioneering integration of Land use type (LU) and Population density (PD) to form the anthropogenic impact parameter (H), enabling assessment of the coupled natural-social system.

The selection of Quanzhou City in Fujian Province as a case study is particularly representative: The city's five-year average per capita water availability was only 856 m^3, as reported in the Quanzhou Water Resources Bulletin (2019–2023), well below the water stress threshold of 1,000 m^3 proposed by the United Nations Food and Agriculture Organization (FAO) (Falkenmark, 1986). Moreover, nitrate exceedance rates in groundwater have reached 57.86% (WHO limit: 50 mg/L), and the proportion of children exposed to health risks is as high as 67.14%. As the starting point of the Maritime Silk Road, Quanzhou's water security holds strategic significance.

This study aims to provide novel methodological support for NVZ delineation through the development and validation of the DITAPH model, thereby offering scientific basis for governmental implementation of surface pollution control and water resource management planning within NVZs. The research outcomes will deliver technical guidance for sustainable water resource management in rapidly urbanizing coastal regions of southeastern China.

1 Overview of the study area

1.1 Physical geography and social economy

Quanzhou is located in southeastern China (117° 34′–119° 05′ E, 24° 30′–25° 56′ N). It consists of land, sea, and islands, with terrain sloping from high elevations in the northwest to low elevations in the southeast, and landforms gradually transitioning from mesas and low mountains to hills, tablelands, and plains. The city has a humid subtropical maritime monsoon climate, with frequent typhoons in summer and autumn. The average annual temperature ranges from 19.5°C to 22°C, while average annual rainfall varies from 1,000 mm to 1,800 mm, increasing from southeast to northwest.

Quanzhou features a dense network of rivers and streams, with the main river flow direction

predominantly from northwest to southeast, controlled by regional geological formations. The aquifer systems comprise Fractured Intrusive Rock Aquifer Units, Weathered Bedrock Fracture Aquifer Units, and Unconsolidated Porous Aquifer Units, with well yield ranging from 10 m^3/d to 1,000 m^3/d. (Fig. 1).

1.2 Geological and hydrogeological conditions

Quanzhou is located within the Fu'an-Nanjing Fracture Zone and the Binhai Fracture Zone. The general tectonic orientation of the region is predominantly north-east, followed by north-west. The stratigraphy in the area is incompletely developed, with exposures of the Upper Jurassic Changlin Formation (J_3c), South Park Formation (J_3n), and Pleistocene (undivided, Q_p), Upper Pleistocene (Q_{p3}), and Holocene (Q_h).

Groundwater in Quanzhou is primarily stored in loose rock pore aquifers, weathered zone pore-fissure aquifers, and bedrock fissure aquifers. Pore water in loose strata is mainly distributed in pre-mountain areas of the coastal plain, mountain basins in the north-central region, and secondary terraces. The lithology consists of sand, gravel, pebbles and wind and sea sand brought by alluvial or flood deposits. The water yield property of these aquifers ranges from poor to medium. Weathering zone pore-fissure water occur in mountains, hills and the piedmont edges of tableland. Lithology is dominated by residual sandy clay loam and gravelly clay loam, with coastal areas characterized by red loam. Groundwater is stored within networks of weathering fissures, generally exhibiting low water quantity and mineralization below 1 g/L.

Bedrock fissure water is present in low mountains, hills and plateaus, plains and basins, occurring as confined groundwater beneath unconsolidated Quaternary deposits. The bedrock are mainly composed of massive volcanic rocks, intrusive rocks and a few layered sedimentary rocks. Water yield is highly heterogeneous, typically poor to very poor, with local areas being moderately rich. Mineralization is generally below 1 g/L.

Groundwater recharge is primarily derived from vertical infiltration of atmospheric precipitation and agricultural irrigation, as well as lateral runoff

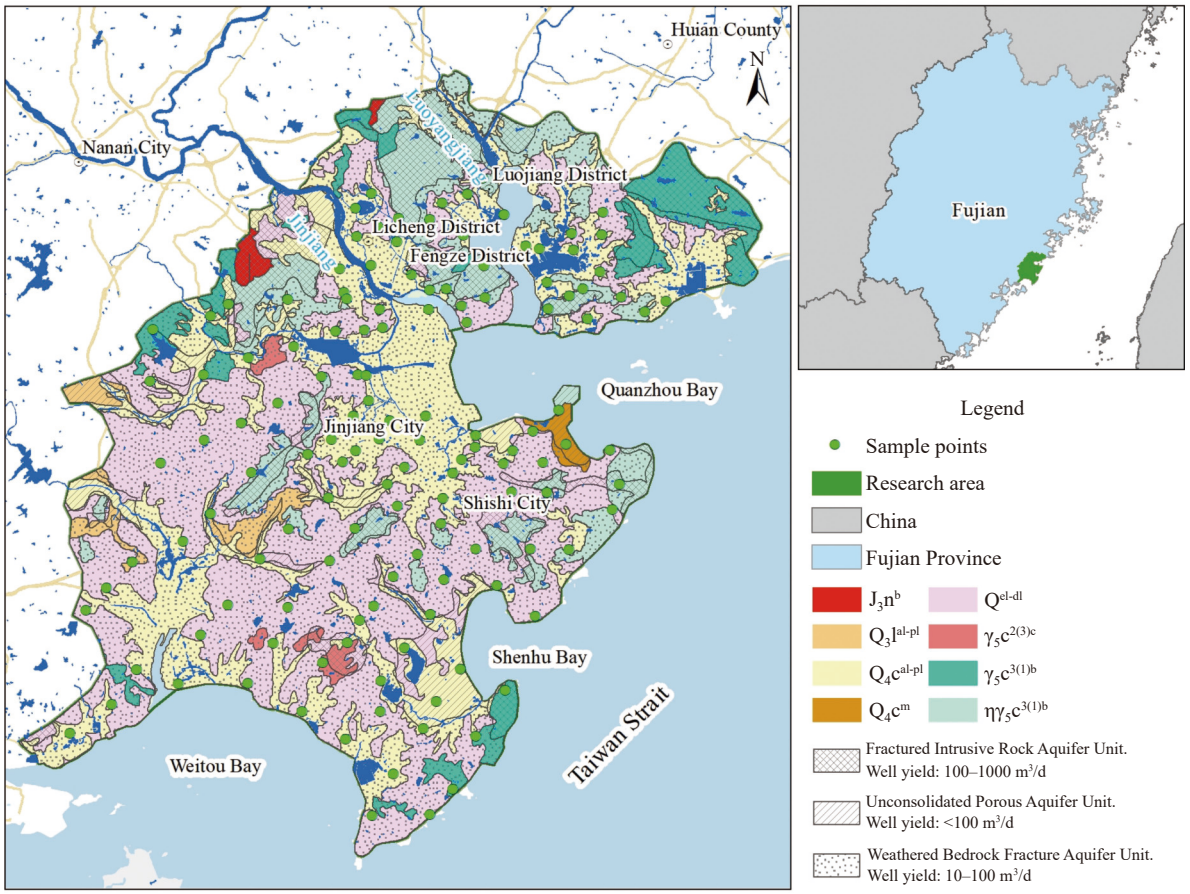

Fig. 1 Location of the research area

from bedrock mountainous areas during the rainy season. The general groundwater flow direction is from the northwest and northeast toward the southeast coast.

2 Materials and methods

2.1 Data source

The GIS-based DITAPH model was used to assess groundwater nitrate vulnerability and delineate NVZs in Quanzhou. The data sources used in the model are detailed in Table 1.

2.2 DITAPH model construction

2.2.1 Assessment parameters

Depth of groundwater (D): Depth of groundwater (D) determines the distance contaminant have to travel to reach the saturated zone and the contact time between contaminants and the surrounding media (Aller et al. 1987; Kumar and Pramod Krishna, 2020). In general, as groundwater depth increases, contaminant migration distance increases, while contaminant concentration decreases due to longer contact time with the surrounding media, leading to reduced aquifer contamination. Groundwater depth data were obtained from 221 observation wells monitored by our team, including information on groundwater depth, surface elevation, and geographic location. A groundwater depth map was interpolated based on the 2020 water-abundance period data.

Impact of vadose zone (I): The seepage flow path is strongly influenced by the type of vadose zone medium, which controls how recharge water reaches the aquifer. The transit time of contaminants, as well as the dilution, adsorption and degradation that occurs during migration, varies according to the medium type. The vadose zone is therefore a critical factor affecting aquifer vulnerability, reflecting the filtering and sorptive capacity for contaminants (Arora et al. 2019; Chakraborty et al. 2022).

Key attributes considered in scoring of the vadose zone medium included: Development of fissures, laminae and cavities of consolidated rock, and particle size, sorting and composition of unconsolidated sediments.

A 1:250,000 geological map of the coastal area of southern Fujian (Deng et al. 2002) was revised to produce a lithological map of the vadose zone, based on the lithological description of the unsaturated strata obtained from collected borehole data.

Topographic slope (T): Whether contaminants run off enter surface runoff or infiltrate the subsurface is determined by terrain slope (Aller et al. 1987). The risk of groundwater contamination increases with decreasing terrain slope, which facilitates recharge water infiltration. To obtain the topographic slope of the study area, a slope map was generated using DEM data provided by NASA (National Aeronautics and Space Administration) via the slope tool in the GIS software.

Aquifer water yield property (A): Aquifer's dilution capacity is influenced by its water yield property. Typically, dilution capacity depends primarily on aquifer thickness, specific yield, and water yield property. When reliable aquifer thickness data are available from abundant boreholes, thickness can effectively reflect dilution capacity. Unfortunately, accurate data on aquifer thickness and specific yield were difficult to obtain from the boreholes collected in this study. Therefore, in this model, aquifer water yield property was selected as the assessment parameter for aquifer dilution capacity, since dilution capacity decreases as water yield deteriorates. Based on data collected from hydrogeologic boreholes and pumping tests, the 1:250,000 hydrogeologic map of the southern coastal area of Fujian (Tao et al. 2002) was revised to produce a map of aquifer water yield properties in the study area.

Table 1 Data Sources for the DITAPH model

Data type		Sources
Depth of groundwater (D)		Manual measurement
Impact of vadose zone lithology (I)		Geological map of the southern coastal area of Fujian
Topographic slope (T)		NASA DEM - National Aeronautics and Space Administration
Aquifer thickness (A)		Hydrogeologic map of the southern coastal area of Fujian
Precipitation (P)		China 1 km Resolution Monthly Precipitation Dataset (1901–2023)
Human Activity (H)	Land use	China multi-period land use land cover data set (CNLUCC)
	Population density	Nighttime Lights Data - National Aeronautics and Space Administration

Precipitation (P): Precipitation is an important climatic parameter affecting aquifer recharge. Precipitation data were used to replace net recharge in the model to avoid duplication and confusion with precipitation and impact of vadose zone. Contaminant levels in phreatic aquifers increase with infiltrating water from rainfall. Annual precipitation was used as the input for this model. These data are derived from the "China 1 km Resolution Monthly Precipitation Dataset (1901–2023) (Peng et al. 2019) ". The dataset is monthly data generated by the Delta Spatial Downscaling Program downscaled in China based on the global 0.5° climate dataset published by CRU (Cimatic Research Unit) and the global high-resolution climate dataset published by WorldClim. Contour map of multi-year average precipitation were generated from 2000–2020 precipitation data through the raster computing tool.

Human activity(H): Two parameters, land use type and population density, were chosen to reflect the anthropogenic impacts on groundwater nitrate contamination. Land use type reflects how humans have transformed and used the land. This determines the type, amount, and intensity of contaminants (Ahmad et al. 2021; Zenebe et al. 2020). Land use type data were manually extracted from the China Multi-period Land Use Land Cover Dataset (CNLUCC) (Xu et al. 2018). Among these land type, urban land, defined as built-up areas, transportation land and industrial land, represents a primary contributor to groundwater nitrate pollution. As a key environmental parameter for identifying human activity intensity, population density directly influences the volume of urban domestic sewage generated. Higher population density correlates with greater sewage discharge, consequently increasing the risk of groundwater nitrate contamination (Ahada and Suthar, 2018). This study classified population density using nighttime lights data published by NASA and NOAA (National Oceanic and Atmospheric Administration) (Levin et al. 2020), applying threshold segmentation to categorize light intensity into five classes (High, Medium, Medium-Low, Low, Very Low), and established a linear regression model (R^2 = 0.78) between light intensity and population density calibrated with census data. Urban land was ultimately divided into five population density tiers: >100 (High Density), 50–100 (Medium Density), 25–50 (Medium-Low Density), 1–25 (Low Density), and ≤1 person/km^2 (Very Low Density). The land use and population density maps were then overlaid to complete the spatial distribution map depicting the integrated intensity of human activities.

2.2.2 Assessment parameter weights and classification

A theoretical weight ranging from 0.5 to 5 was assigned to each DITAPH assessment parameter according to the magnitude of their impact on vulnerability, with a weight of 5 for the highest impact and a weight of 0.5 for the lowest impact. The theoretical weights of the parameters, presented in Table 2, were determined based on a synthesis of relevant existing research findings (Deka et al. 2025; George et al. 2025; Iqbal et al. 2024; Zhong, 2005) and the expert scoring method, where five hydrogeological experts independently scored each parameter, and the final weight was calculated as the mean of their scores.

2.2.3 Calculation of the DITAPH index

The DITAPH index was calculated using Equation (1):

$$DI = D_r \times D_w + I_r \times I_w + T_r \times T_w + A_r \times A_w + P_r \times P_w + H_r \times H_w \quad (1)$$

In Equation (1), DI represents the DITAPH index, and r and w are the rating scores and weights assigned to each parameter. Higher DI values indicate greater groundwater vulnerability.

2.3 Groundwater Nitrate Vulnerability Assessment

2.3.1 Sensitivity analysis

Research has shown that the weighting of the vulnerability index (DI) varies depending on the

Table 2 Theoretical weights assigned to DITAPH parameters

Parameter	D	I	T	A	P	H
Theoretical weight	2.5	0.5	1.5	2	0.5	5

Note: The weight values were dynamically calibrated through sensitivity analysis. Each of the six assessment parameters of the DITAPH model was divided into ranges or categories, and then rating scores were assigned to each range/category according to the magnitude of the impact of the different ranges/categories on groundwater vulnerability (Fig. 2), with reference to the DRASTIC index scoring method proposed by Aller (Aller et al. 1987) and the Modified DRASTIC index scoring method proposed by Zhong (Zhong, 2005). Each of the assessment parameters is rated on a scale of 1 to 10, with higher scores indicating greater impact of the parameter on groundwater vulnerability.

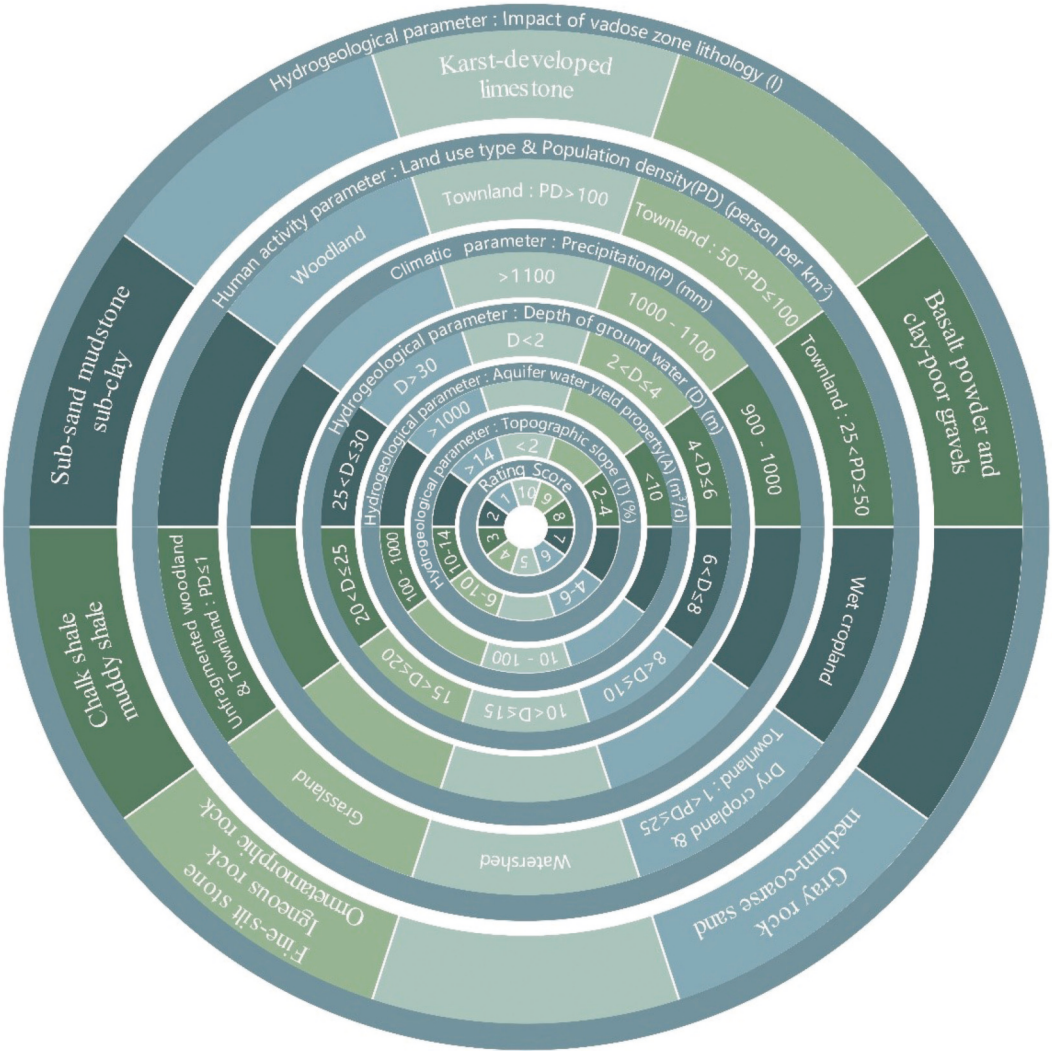

Fig. 2 Classes and ratings for DITAPH parameters

study area (Babiker et al. 2005). Single-parameter sensitivity analysis was conducted to compare the relationship between the theoretical weights and the effective weights of the vulnerability assessment parameters. The effective weights are influenced by the theoretical weights and ratings of each individual assessment parameter (Javadi et al. 2011; Sidibe and Lin, 2018). The effective weights (W) was calculated using Equation (2):

$$W = \left(\frac{P_r \times P_w}{DI}\right) \times 100\% \quad (2)$$

In Equation (2), W is the effective weight of each parameter, P_r is the rating score, P_w is the theoretical weight, and DI is the vulnerability index value.

2.3.2 Vulnerability Classification and NVZs Delineation

Based on the results of the sensitivity analysis, the weights of the DITAPH model assessment parameters were corrected and the DI values were recalculated. Groundwater nitrate vulnerability was then categorized into four classes: Low, relatively low, relatively high, and high vulnerability zones (Khosravi et al. 2018). NVZ maps were generated using the quartile method.

2.3.3 DITAPH model validation

To verify the accuracy of NVZ delineation, correlation analysis was conducted between DITAPH index (DI) and measured NO_3^- concentration from 139 groundwater samples. The correlation was expressed as Pearson's correlation coefficient (R), calculated using Equation (3):

$$R = \frac{n\left(\sum \rho \times DI\right) - \left(\sum \rho\right)\left(\sum DI\right)}{\sqrt{n\sum \rho^2 - \left(\sum \rho\right)^2}\sqrt{n\sum DI^2 - \left(\sum DI\right)^2}} \quad (3)$$

In Equation (3), R is the Pearson correlation coefficient, n is the number of data points, ρ is the nitrate concentration (mg/L), and DI is the DITAPH index value.

3 Results and discussion

3.1 Thematic maps

3.1.1 Depth of groundwater (D)

The depth of groundwater in the study area ranges from 0.34 m to 14.92 m and is distributed in grades of 5–10 (Fig. 3a). The predominant groundwater depth ranges from 2 m to 6 m, covering 66.2% of the total area. The areas classified as grades 8 and 9 cover 487.5 km^2 and 410.6 km^2, respectively, and are mainly located near the Jinjiang River estuary and in the eastern part of Nan'an City. Grade 7 (6–8 m) occurs mainly in the eastern Luojiang River estuary and the northern part of Jinjiang City, accounting for 18.3% of the total area. The proportions of grade 5, 6 and 10 range from 2% to 8%, representing relatively small area.

3.1.2 Impact of vadose zone lithology (I)

The vadose zone lithology in the study area is classified into six grades (2, 3, 4, 6, 8, and 10) (Fig. 3b). Grades 2 (sub-sand, mudstone or sub-clay) and 4 (chalk shale or muddy shale) are widely distributed across the study area, covering 555.2 km^2 and 492.8 km^2, respectively, and accounting for 40.9% and 36.3% of the total area. Grade 8 (basalt powder or clay-poor gravels) covers 295.0 km^2, accounting for 21.7% of the total area, and is mainly distributed in the north and north-east plains, with only sporadic occurrences in the southern plains.

3.1.3 Topographic slope (T)

The study area is predominantly flat, with slopes ranging from 0% to 73.8%, and is divided into five grades: 2, 4, 6, 8, and 10 (Fig. 3c). Grade 8 (2% < T ≤ 4%) and 10 (T ≤ 2%) are the most dominant, covering 439.4 km^2 and 432.3 km^2, respectively, and accounting for 32.4% and 31.8% of the total area.

3.1.4 Aquifer water yield property (A)

The aquifer water yield property in the study area

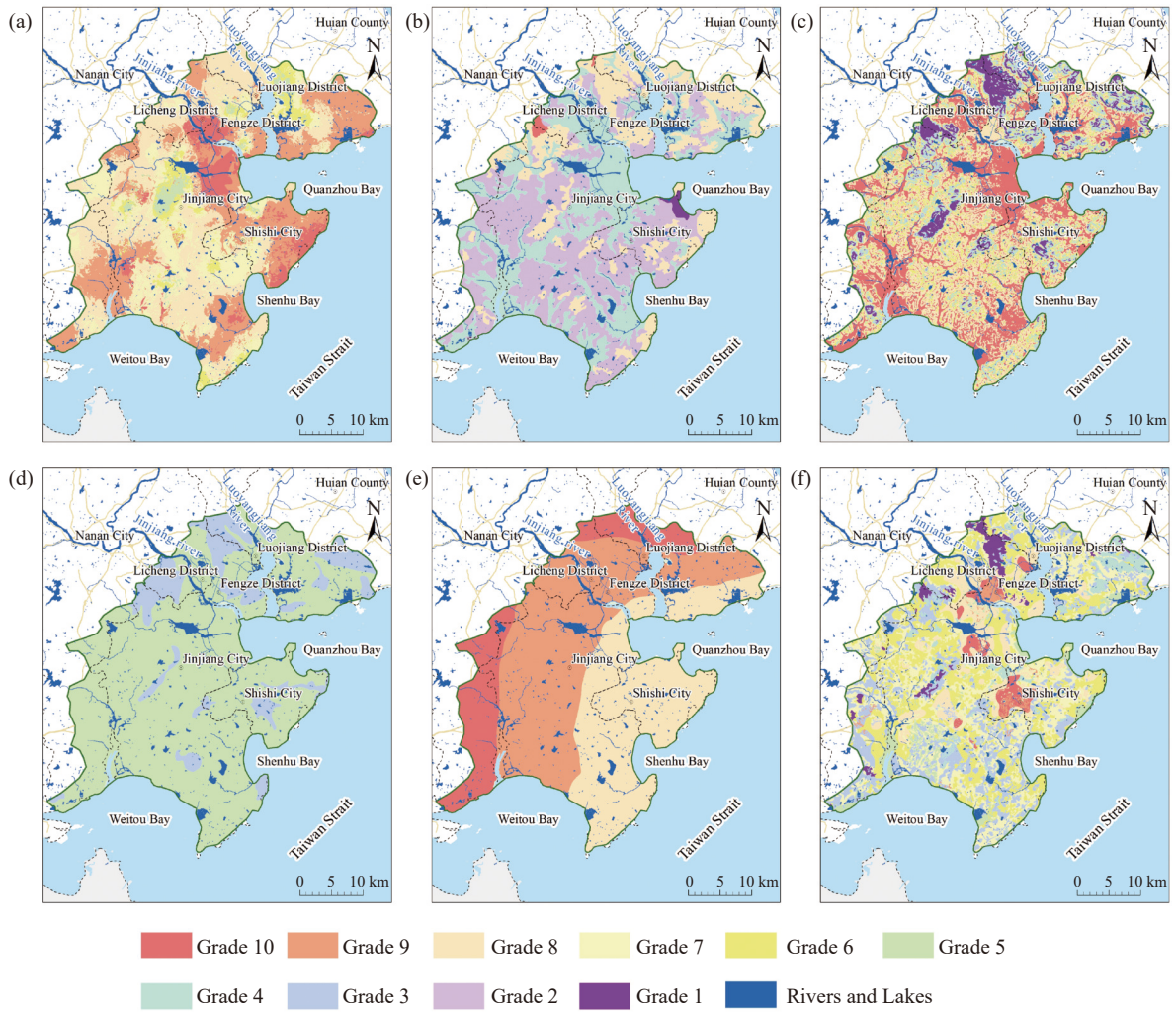

Fig. 3 Thematic maps of assessment parameters in the DITAPH model: (a) Depth of groundwater (D); (b) Vadose zone lithology (I); (c) Topographic slope (T); (d) Aquifer water yield property (A); (e) Precipitation (P); (f) Human activity (H)

ranges from weak to moderate, and is divided into two grades: 3 and 5 (Fig. 3d). Grade 5 (10–100 m^3/d) is widely distributed, covering 84.8% of the total area, while Grade 3 (100–1000 m^3/d) is mainly concentrated in the northern premontane zone.

3.1.5 Precipitation(P)

The study area receives abundant precipitation that gradually decreases from the northwest to the southeast. The average annual precipitation ranges over the years from 946 mm to 1,221 mm and was classified into three grades (grade 8, 9, and 10) (Fig. 3e). Grade 9 (1,000 mm < P ≤ 1,100 mm) and 8 (900 mm < P ≤ 1,000 mm) are the dominant categories in the region, with areas of 625.4 km^2 and 503.2 km^2, accounting for 46.1% and 37.1%, respectively.

3.1.6 Human activity(H)

Land use in the study area is classified into seven categories: Wet cropland, dry cropland, watershed, grassland, unfragmented woodland, woodland and townland (Fig. 4a). Townland is further classified into five grades according to population density (persons/km^2): >100, 50–100, 25–50, 1–25, and ≤1 (Fig. 4b). The thematic human activities map (Fig. 3f), derived from the overlay of land use and population density, is divided into 9 grades (1, 3, 4, 5, 6, 7, 8, 9 and 10).

Grade 6 (dry cropland or townland with a population density of 1–25 persons/km^2), Grade 7 (wet cropland) and Grade 3 (unfragmented woodland or townland with a population density of ≤1 persons/km^2) are the most widely distributed, covering 27.6%, 24.5% and 21% of the total area, respectively. Grade 8 (townland with a population density of 25–50 persons/km^2) accounts for 10.1% of the total area. Grade 5 (watershed), Grade 4 (grassland), and Grade 1 (woodland) occupy smaller areas, accounting for 5.6%, 4.6%, and 2.7%, respectively. The proportion of townland with a population density exceeding 50 persons/km^2 is 3.9%, mainly concentrated in the built-up areas of Quanzhou, Jinjiang and Shishi City.

3.2 Sensitivity analysis

The results of the sensitivity analysis indicated that the effective weights of groundwater depth, topographic slope and precipitation (26.2%, 15.2% and 5.6%) were higher than their theoretical weights (20.8%, 12.5% and 4.2%). In contrast, the effective weights of water yield property of aquifer, human activity and vadose zone lithology (12.5%, 38.1% and 2.4%) were lower than their corresponding theoretical weights (16.7%, 41.7% and 4.2%). Overall, the relative influence of the DITAPH model parameters on groundwater nitrate vulnerability, in descending order, was human activities, depth of groundwater, topographic slope, aquifer water yield property, precipitation, and vadose zone lithology. The effective weights of the DITAPH model parameters were derived from the sensitivity analysis (Fig. 5).

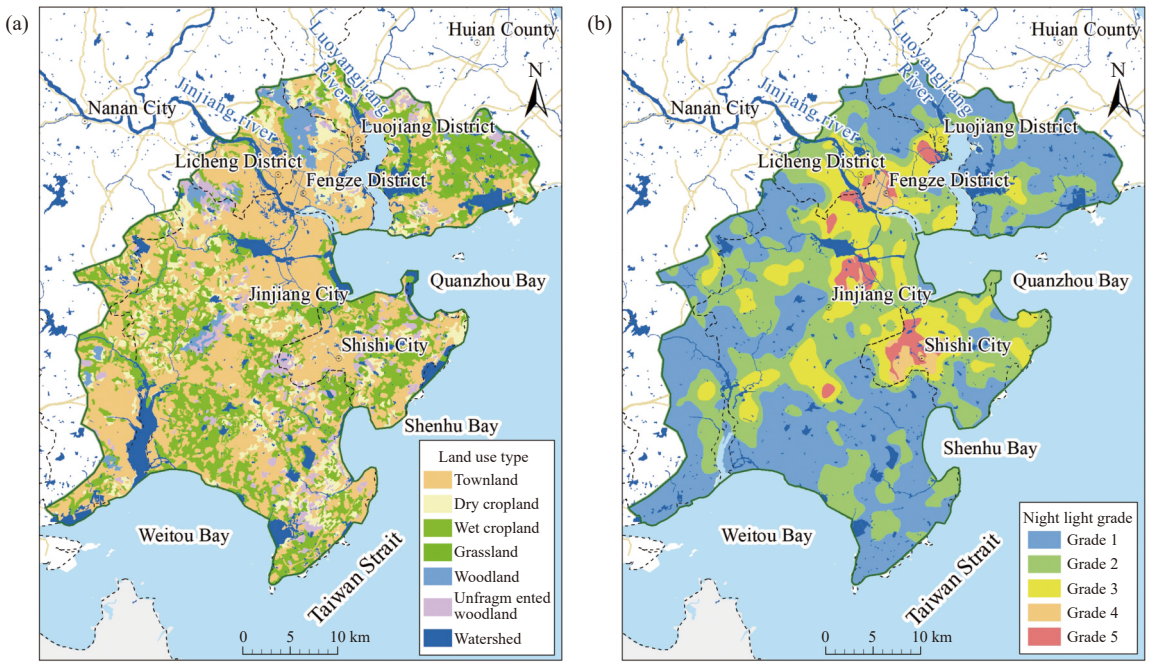

Fig. 4 Thematic map of human activity parameters in the DITAPH model: (a) Land use map (LU); (b) nighttime lighting grading map (NTL)

3.3 Groundwater nitrate vulnerability classification and NVZs delineation

By recalculating the DI using the modified weights from Equation (1), the values ranged from 33 to 106.5. Based on the hydrogeological characteristics of the study area, the vulnerability levels were classified using the quartile method into four categories: <55 (Low), 55–75 (Moderate), 75–95 (High), and ≥95 (Very High). Accordingly, four Nitrate Vulnerability Zones (NVZs) were delineated: Low Zones (LZs), Rs (RHZs), High Zones (HZs) (Fig. 6). LZs are mainly located in mountainous areas characterized by steep topography, deeper groundwater depth, and predominantly woodland land use. RLZs are widely distributed across the study area, where land use is dominated by other forest land (49.45%), followed by dry

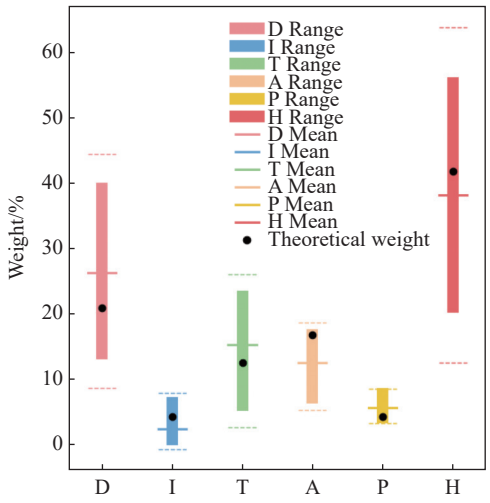

Fig. 5 Comparison between theoretical weight and effective weight of DITAPH model

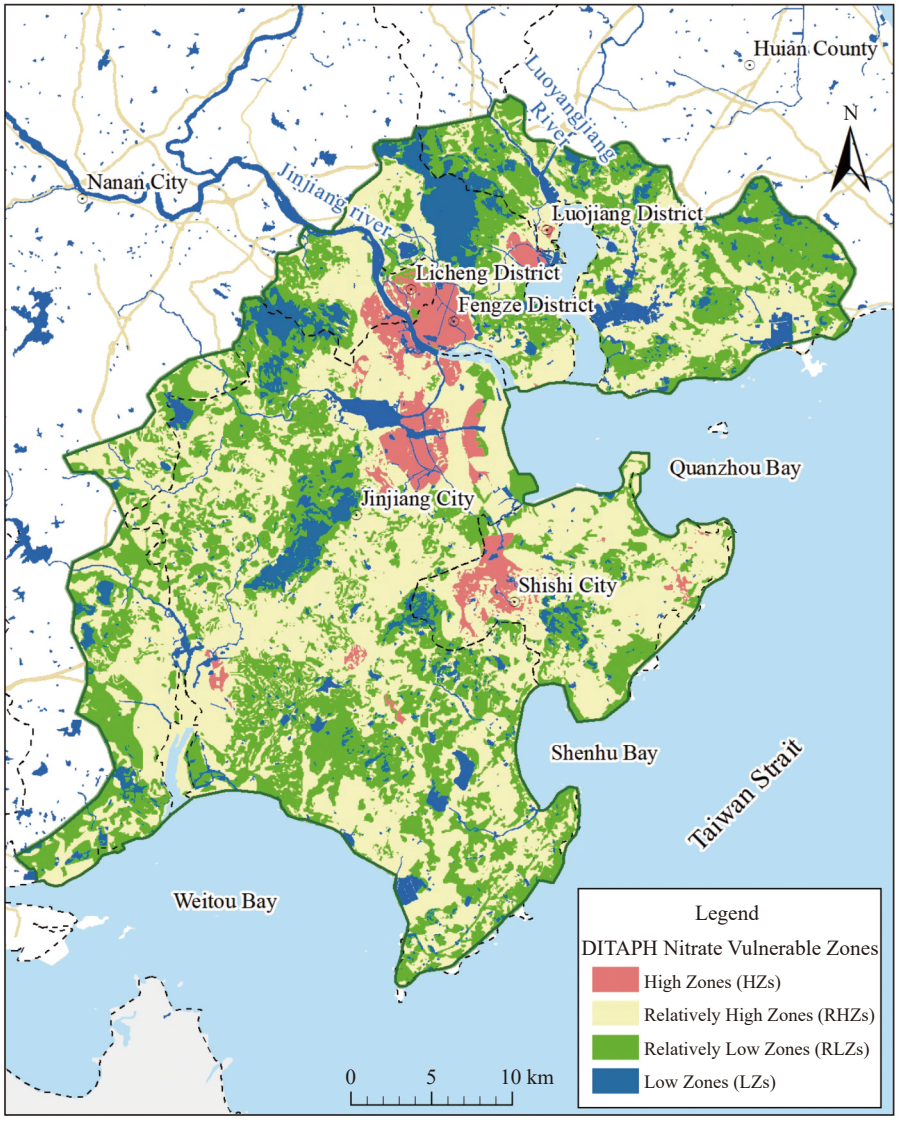

Fig. 6 Spatial Distribution of NVZs Delineated by the DITAPH Model

land (26.29%). RHZs are mainly concentrated in agricultural zones, with 33.87% and 42.79% of their area classified as wet and dry croplands, respectively. These zones are further characterized by gentle topographic slopes, low aquifer water yield properties, and shallow groundwater depths. Subzones with groundwater levels of 4–8 m and <4 m account for approximately 53% and 34% of the area, respectively. HZs are primarily concentrated in urban areas, with 62% distributed in areas having population densities exceeding 50 persons/km^2 – mainly in Fengze District, Shishi City and Jinjiang City. Similar to RHZs, these zones exhibit shallow groundwater depth, low topographic gradients, and poor water yield property.

The areal extent of RHZs (53.74%) is significantly greater than that of HZs (4.86%). This disparity is mainly due to the large proportion of agricultural land (40.25% of the study area, including both wet and dry croplands) and the high annual nitrogen fertilizer application rate (297 kg/ha), which exceeds the national average of 280 kg/ha (Fu et al. 2023). Such intensive fertilization increases the risk of nitrate leaching into groundwater. In contrast, the smaller extent of urban HZs is partly attributed to improved municipal wastewater treatment rates (60%) (QMEEB, 2021), which have reduced overall pollution loads. However, localized areas, such as Fengze District, still exhibit high nitrate vulnerability due to limited sewer network coverage (<50%) and delays in the centralized sewage collection.

The comparison of hydrogeological and climatic conditions and anthropogenic characteristics of groundwater NVZs at different levels (Table 3) shows that both natural conditions and anthropogenic activities jointly influence groundwater nitrate vulnerability. A shared characteristic of the HZs and RHZs is that they are predominantly affected by human activities, followed by the influence of groundwater depth and topographic slope. Specifically, the RHZs are mainly influenced by agricultural practices, underscoring the urgent need to restrict the use of nitrogen fertilizers and animal manure. In contrast, the HZs are primarily affected by domestic and industrial sewage from urban areas, emphasizing the importance of improving wastewater treatment efficiency and strengthening the management of wastewater discharges.

3.4 Validation

3.4.1 Distribution of nitrate concentration in groundwater

Among the 139 groundwater samples collected (distributed as follows: RLZs: 48, RHZs: 85, HZs: 6), NO_3^- concentration ranged from 2.18 mg/L to 193.1 mg/L. The "Standard for groundwater quality" (GB/T 14848—2017) was used as the evalua-

Table 3 Characteristic parameters of NVZs

Vulnerability class		LZs	RLZs	RHZs	HZs
Index value		DI<55	55≤DI<75	75≤DI<95	DI≥95
Area (km^2)		80.85	480.98	729.42	66.03
Area percentage (%)		5.96	35.44	53.74	4.86
Hydrogeological parameters	**D**	4–8 m: 72% of area 2–4 m: 12% of area	4–8 m: 59% of area 2–4 m: 28% of area	4–8 m: 53% of area 2–4 m: 34% of area	4–8 m: 24% of area 2–4 m: 63% of area
	I	Mainly granite, tuff lava, followed by clay, clayey sand, sandy clay	Mainly clay, clayey sand, sandy clay, silty clay, followed by granite, tuff lava	Mainly clays, clayey sands, sandy clays and silt and fine sands	Mainly fine sand and clay
	T	> 20%: 79% of area	4–10%: 38% of area ≤4%: 47% of area	≤4%: 80% of area	≤4%: 97% of area
	A	100–1,000 m^3/d: 69% of area	10–100 m^3/d: 78% of area	10–100 m^3/d: 94% of area	10–100 m^3/d: 99% of area
	P	>1,000 mm: 86% of area	900–1,000: 79% of area	900–1,000: 85% of area	1,000–1,100 mm: 65% of area 900–1,000 mm: 35% of area
Climatic parameter	**P**	>1,000 mm: 86% of area	900–1,000: 79% of area	900–1,000: 85% of area	1,000–1,100 mm: 65% of area 900–1,000 mm: 35% of area
Human activity parameters	**H**	unfragmented woodland: 43% of area woodland: 36% of area	Unfragmented woodland: 49% of area dry cropland: 26% of area	wet cropland: 43% of area dry cropland: 34% of area	Mainly townland, with a population density of >50 persons/km^2: 62% of area

tion criterion. Samples from the RLZs exhibited NO_3^- concentrations ranging from 2.18 mg/L to 87.56 mg/L, with a mean value of 31.39 mg/L. All but one sample met the Class III water quality standard, with the proportions of Class I, Class II and Class III water being 18.75%, 27.08% and 52.08%, respectively.

In the RHZs, NO_3^- concentrations ranged from 24.37 mg/L to 140.7 mg/L, with a mean value of 69.97 mg/L. Approximately 29.41% of the samples exceeded the Class III standard limit. In the HZs, NO_3^- concentrations ranged from 75.37 mg/L to 193.1 mg/L, with a mean value of 132.51 mg/L, and 50% of the samples exceeded the Class III limit (Table 4 and Fig. 7).

3.4.2 Correlation analysis validation

Pearson's correlation analysis revealed a linear relationship between the DITAPH index (DI) and groundwater nitrate concentration ($\rho(NO_3^-)$), with a correlation coefficient R of 0.63 (Fig. 8), indicating a significant positive correlation (NO_3^-) ($P \leq 0.01$). These results confirm the reliability of the

Table 4 Distribution of nitrate concentration in groundwater

Vulnerability Class	Samples	Proportion of each groundwater quality class				
		Ⅰ	Ⅱ	Ⅳ	Ⅳ	Ⅴ
HZs	6	16.67%	0.00%	33.33%	33.33%	16.67%
RHZs	85	0.00%	0.00%	70.59%	22.35%	7.06%
RLZs	48	18.75%	27.08%	52.08%	2.08%	0.00%

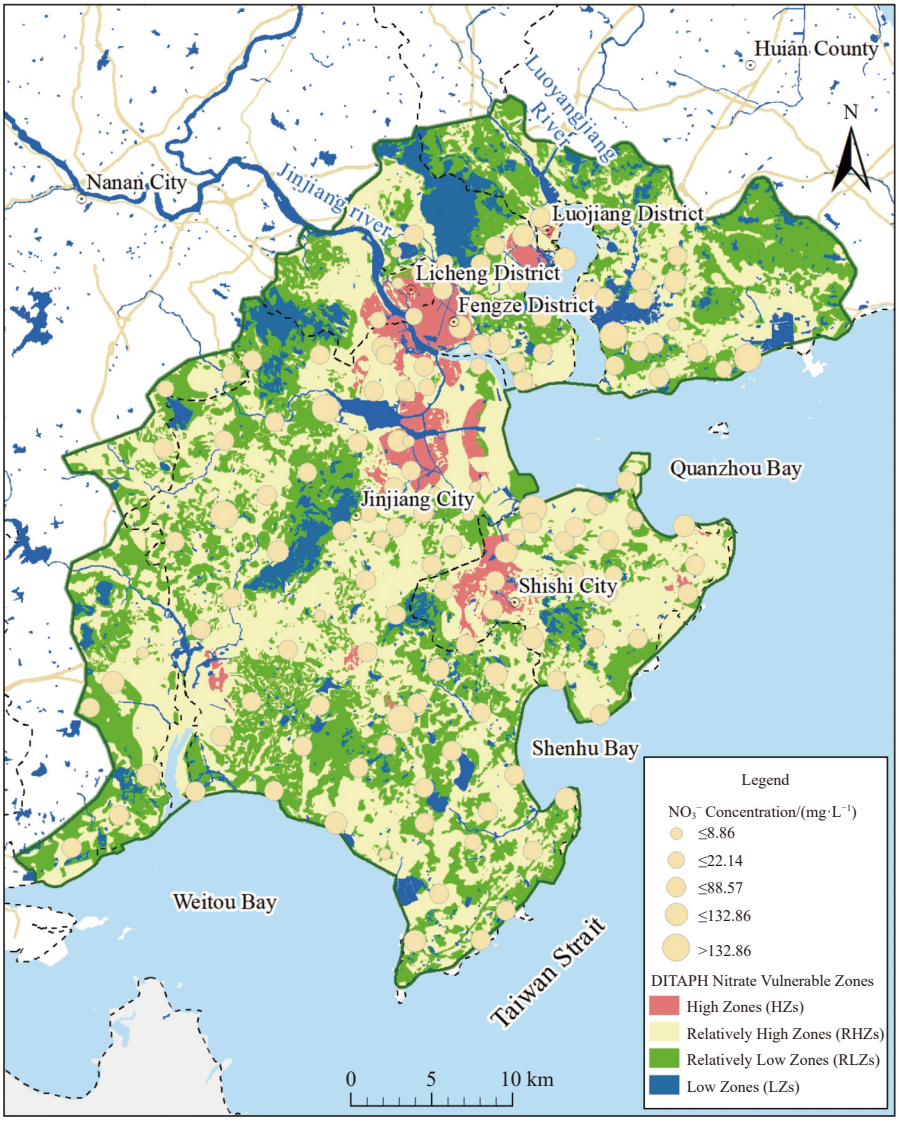

Fig. 7 Spatial distribution of groundwater samples across the NVZs delineated using the DITAPH Model

DITAPH model for groundwater nitrate vulnerability zoning.

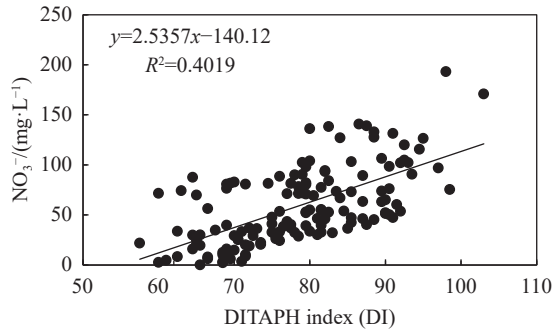

Fig. 8 Linear relationship between DITAPH Index (DI) and groundwater nitrate concentration (NO_3^-)

4 Discussion

4.1 Sensitivity mechanisms of DITAPH parameters

The results demonstrate that human activities (H) exert the highest influence weight on groundwater nitrate vulnerability (effective weight 38.1%), which strongly correlates with Quanzhou's rapid urbanization and agricultural intensification. In the southeastern plains (economic core zone), high population density (>50 persons/km^2) and insufficient sewage collection coverage (current treatment rate <70%) result in direct infiltration of domestic and industrial wastewater. Meanwhile, in the northwestern agricultural areas, long-term excessive nitrogen fertilizer application (cropland accounting for 78.3% of total farmland) intensifies nitrate leaching risks. This finding aligns with research in Punjab, India (Ahada and Suthar, 2018), where anthropogenic parameters (e.g., land use) contribute more significantly to vulnerability than natural parameters in agriculturally dominated regions.

Additionally, the interaction between topographic slope (T) and depth of groundwater (D) warrants attention: In flat plains with gentle slopes (<4%) and shallow aquifers (<4 m) (e.g., Jinjiang River estuary), short pollutant retention time and weak dilution capacity lead to high-vulnerability zones. Conversely, hilly areas with steeper slopes (>10%) (e.g., North Luojiang River) exhibit reduced groundwater contamination risks due to runoff-dominated pollutant transport. Such interactions suggest that future model optimization should incorporate nonlinear parameter relationships to better characterize spatial variability in vulnerability under complex hydrogeological conditions.

4.2 Comparative advantages over DRASTIC model

Compared to the conventional DRASTIC model, DITAPH offers notable improvements in assessment efficiency and practical applicability through the following enhancements:

(1) Reduced parameter redundancy: DITAPH eliminates overlapping parameters in DRASTIC (e.g., aquifer media and hydraulic conductivity), replacing problematic net recharge (R) with readily available precipitation data (P) to address data scarcity (Chakraborty et al. 2022).

(2) Enhanced anthropogenic quantification: By integrating land use and population density, DITAPH directly reflects spatiotemporal variations in agricultural fertilization and urban sewage discharge. For instance, high-vulnerability zones (DI ≥95) overlap significantly with urban built-up areas (62%), whereas DRASTIC may underestimate pollution risks in such regions due to its neglect of anthropogenic parameters (Arauzo, 2017).

(3) Dynamic weight calibration: Theoretical weights are adjusted through single-parameter sensitivity analysis (e.g., H reduced from 41.7% to 38.1%), mitigating subjective assignment bias, consistent with the concept of "data-driven weight calibration" (Javadi et al. 2011).

Fig. 9 presents the DRASTIC NVZs (data sourced from the Fujian Provincial Geological Survey Institute). Table 5 compares the spatial distribution characteristics of water samples within NVZs delineated by the two models. The DITAPH model demonstrates significant advantages over the DRASTIC model: 96.55% of contaminated water samples (quality class IV and V) in the DITAPH model are concentrated in HZs and RHZs, whereas the traditional model identifies only 24.14%. Simultaneously, contaminated samples in RLZs under DITAPH account for merely 2.08%, substantially lower than the 25.88% contamination rate in the traditional model. These results indicate the superior classification accuracy of the DITAPH model. Furthermore, DITAPH exhibits a logically consistent risk gradient. The proportions of contaminated water decrease progressively across vulnerability zones (HZs: 50.00%; RHZs: 29.41%; RLZs: 2.08%). In contrast, the traditional model displays risk inversion, with RLZs exhibiting a higher contamination rate than HZs. These results confirm that by replacing conventional parameters with precipitation (P) and human activity (H), the DITAPH

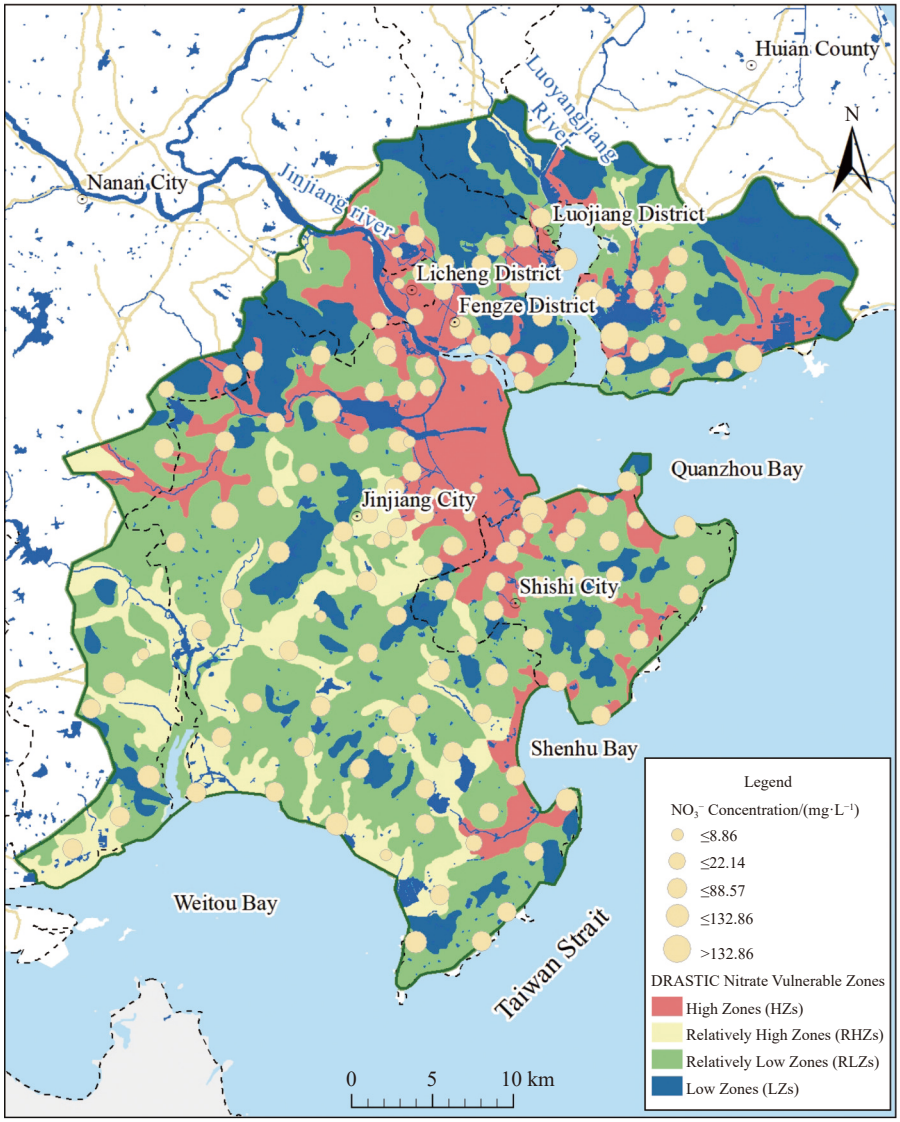

Fig. 9 Spatial distribution characteristics of groundwater samples within NVZs delineated by the DRASTIC model

Table 5 Comparison of groundwater quality distribution within NVZs as delineated by the DRASTIC and DITAPH models

Classification method	Vulnerability class	Samples	Groundwater quality class/%					Compliant water	Contaminated water	Proportion of contaminated water
			Ⅰ	Ⅱ	Ⅲ	Ⅳ	Ⅴ	Class (I - III)	Class (IV - V)	
DRASTIC	HZs	35	5	6	18	5	1	29	6	17.14%
	RHZs	19	2	2	14	0	1	18	1	5.26%
	RLZs	76	3	5	47	16	5	55	21	27.63%
	LZs	9	0	0	8	1	0	8	1	11.11%
DITAPH	HZs	6	1	0	2	2	1	3	3	50.00%
	RHZs	85	0	0	60	19	6	60	25	29.41%
	RLZs	48	9	13	25	1	0	47	1	2.08%
	LZs	0	0	0	0	0	0	0	0	-

model more directly traces nitrate origins and better reflects contamination transport mechanisms through its structural framework.

4.3 Implications for groundwater management

The NVZs delineation results provide practical guidance for targeted groundwater management in Quanzhou:

(1) High-vulnerability zones (urban belts): Prioritize the expansion of sewage network (current treatment rate < 70%) and enforce stricter standards for industrial wastewater discharge.

(2) Moderate-vulnerability zones (agricultural belts): Promote the adoption of slow-release fertilizer technologies and establish nitrogen application thresholds in accordance with the EU Nitrates Directive (91/676/EEC) (Monteny, 2001).

(3) Natural background protection (low-vulnerability zones, e.g., forested areas): Restrict mining and tourism development to preserve aquifer integrity.

4.4 Model limitations and future directions

Although DITAPH has demonstrated good performance in Quanzhou's plains, several limitations should be considered:

(1) Spatial scale dependency: The 1 km-resolution model may overlook small-scale pollution sources (e.g., livestock farms); integrating high-resolution remote sensing and field monitoring is recommended.

(2) Heterogeneous aquifer applicability: In fractured bedrock aquifers (e.g., northern study area), spatial variability in hydraulic conductivity may lead to underestimation of vulnerability under DITAPH's homogenization assumptions.

(3) Dynamic process exclusion: Seasonal variations in precipitation and irrigation-induced parameter changes are not accounted for; coupling DITAPH with hydrological models could improve spatiotemporal continuity in vulnerability assessment.

5 Conclusions

This study presents the development of the DITAPH model, which integrates groundwater dynamics with human activities to overcome limitations of traditional models, such as parameter redundancy and insufficient quantification of anthropogenic impacts. The model was applied to assess groundwater nitrate vulnerability and delineate Nitrate Vulnerable Zones (NVZs) in the plain area of Quanzhou. The main conclusions are as follows:

(1) Spatial distribution of vulnerability: Application of the DITAPH model revealed that groundwater nitrate vulnerability in Quanzhou is predominantly classified as relatively high or high. Relatively high zones were primarily distributed across agricultural areas, representing the largest proportion of the study area. High zones were concentrated in densely populated urban centers, including Fengze District, Shishi City, and Jinjiang City. In contrast, relatively low zones and low zones were mainly located in the northwestern mountainous region, characterized by steeper slopes, deeper groundwater levels, and dominant forest land use. Sensitivity analysis identified human activity was the most influential factor, followed by the depth to groundwater and topographic slope.

(2) Model performance and advantages: The DITAPH model demonstrated clear superiority over the conventional DRASTIC model. The parameter system was refined by replacing net recharge with precipitation and integrating land use type and population density into a human activity parameter. Parameter weights were calibrated via sensitivity analysis, reducing both parameter redundancy and subjectivity. Validation confirmed a significant positive correlation between the DITAPH index and measured nitrate concentrations. Furthermore, the distribution of contaminated water samples across NVZ categories exhibited a consistent and logical gradient. Overall, the DITAPH model achieved significantly higher classification accuracy than the DRASTIC model, substantiating its enhanced reliability and practical utility.

(3) Implications for groundwater management: Based on the DITAPH assessment and sensitivity analysis, a zonal and hierarchical strategy for controlling groundwater nitrate contamination in Quanzhou is recommended. In high vulnerability zones, urban sewage treatment should be enhanced to increase wastewater treatment coverage. In relatively high vulnerability zones, precision fertilization informed by soil testing should be implemented, supported by slow-release fertilizers and nitrification inhibitors. For relatively low and low vulnerability zones, management should focus on establishing groundwater Ecological Conservation Redlines (ECRLs), prohibiting new sources of contamination, and implementing a monitoring network for dynamic early-warning.

Acknowledgments

This study was supported by the National Key Research and Development Program of China (No. 2022YFF1301301), the Natural Science Foundation of Xiamen Municipality (No. 3502Z20247 2047), and the Geological Survey Program of China Geological Survey (DD20190303).

References

Abascal E, Gómez-Coma L, Ortiz I, et al. 2022. Global diagnosis of nitrate pollution in groundwater and review of removal technologies. Science of The Total Environment, 810: 152233. DOI：10.1016/j.scitotenv.2021.152233.

Ahada CPS, Suthar S. 2018. A GIS based DRASTIC model for assessing aquifer vulnerability in Southern Punjab, India. Modeling Earth Systems and Environment, 4: 635−645. DOI：10.1007/s40808-018-0449-6.

Ahmad W, Iqbal J, Nasir MJ, et al. 2021. Impact of land use/land cover changes on water quality and human health in district Peshawar Pakistan. Scientific Reports, 11: 16526. DOI：10.1038/s41598-021-96075-3.

Aller L, Bennett T, Lehr J, et al. 1987. DRASTIC: Standardized system for evaluating groundwater pollution potencial using hydrogeologic settings. Journal of the Geological Society of India: 29. DOI: 10.17491/jgsi/1987/290112

Arauzo M. 2017. Vulnerability of groundwater resources to nitrate pollution: A simple and effective procedure for delimiting Nitrate Vulnerable Zones. Science of The Total Environment, 575: 799−812. DOI：10.1016/j.scitotenv.2016.09.139.

Arauzo M, Martínez-Bastida JJ. 2015. Environmental factors affecting diffuse nitrate pollution in the major aquifers of central Spain: Groundwater vulnerability vs. groundwater pollution. Environmental Earth Sciences, 73: 8271−8286. DOI：10.1007/s12665-014-3989-8.

Arauzo M, Valladolid M, Andries DM. 2022. Would delineation of nitrate vulnerable zones be improved by introducing a new parameter representing the risk associated with soil permeability in the Land Use–Intrinsic Vulnerability Procedure? Science of The Total Environment, 840: 156654. DOI:10.1016/j.scitotenv.2022.156654

Arora B, Dwivedi D, Faybishenko B, et al. 2019. Understanding and predicting vadose zone processes. Reviews in Mineralogy and Geochemistry, 85: 303−328. DOI：10.2138/rmg.2019.85.10.

Babiker I, Mohamed M, Hiyama T, et al. 2005. A GIS-based DRASTIC model for assessing aquifer vulnerability in Kakamigahara Heights, Gifu Prefecture, central Japan. Science of The Total Environment, 345: 127−140. DOI：10.1016/j.scitotenv.2004.11.005.

Chakraborty B, Roy S, Bera A, et al. 2022. Groundwater vulnerability assessment using GIS-based DRASTIC model in the upper catchment of Dwarakeshwar river basin, West Bengal, India. Environmental Earth Sciences, 81: 2. DOI：10.1007/s12665-021-10002-3.

Chilaule SM, Vélez-Nicolás M, Ruiz-Ortiz V, et al. 2023. Assessment of intrinsic vulnerability using DRASTIC vs. Actual nitrate pollution: The case of a detrital aquifer impacted by intensive agriculture in Cádiz (Southern Spain). Agriculture, 13: 1082. DOI：10.3390/agriculture13051082.

Deka D, Ravi K, Nair AM. 2025. Impact of urbanisation on groundwater vulnerability in shallow aquifer system of Assam: A DRASTIC approach. Urban Climate, 59: 102299. DOI：10.1016/j.uclim.2025.102299.

Deng D, Lai S, Deng Y. 2002. 1: 250, 000 geological map of the coastal area of southern Fujian.

Falkenmark M. 1986. Fresh water. Time for a modified approach - Eau douce. Le moment d'un changement d'approche. Ambio, 15(4): 192−200.

Fu JJ, Le XC. 2025. Improving groundwater vulnerability assessment using machine learning. Journal of Environmental Sciences, 153: 6−9. DOI：10.1016/j.jes.2024.12.024.

Fu SM, Wang KF. 2023. Quanzhou Statistical Yearbook 2023. China Statistics Press, Beijing. https://tjj.quanzhou.gov.cn/

George NJ, Agbasi OE, Umoh AJ, et al. 2025. Enhanced contamination risk assessment for aquifer management using the geo-resistivity

and DRASTIC model in alluvial settings. Cleaner Water, 3: 100060. DOI：10.1016/j.clwat.2024.100060.

Gutiérrez M, Biagioni RN, Alarcón-Herrera MT, et al. 2018. An overview of nitrate sources and operating processes in arid and semiarid aquifer systems. Science of the Total Environment, 624: 1513−1522. DOI：10.1016/j.scitotenv.2017.12.252.

Hamza SM, Ahsan A, Imteaz MA, et al. 2015. Accomplishment and subjectivity of GIS-based DRASTIC groundwater vulnerability assessment method: A review. Environmental Earth Sciences, 73: 3063−3076. DOI：10.1007/s12665-014-3601-2.

Iqbal MA, Salam MA, Nur-E-Alam M, et al. 2024. Monitoring groundwater vulnerability for sustainable water resource management: A DRASTIC-based comparative assessment in a newly township area of Bangladesh. Groundwater for Sustainable Development, 27: 01373. DOI：10.1016/j.gsd.2024.101373.

Javadi S, Kavehkar N, Mohammadi K, et al. 2011. Calibrating DRASTIC using field measurements, sensitivity analysis and statistical methods to assess groundwater vulnerability. Water International, 36: 719−732. DOI：10.1080/02508060.2011.610921.

Khosravi K, Sartaj M, Tsai FT-C, et al. 2018. A comparison study of DRASTIC methods with various objective methods for groundwater vulnerability assessment. Science of The Total Environment, 642: 1032−1049. DOI：10.1016/j.scitotenv.2018.06.130.

Kong XK, Zhang ZX, Wang P, et al. 2022. Transformation of ammonium nitrogen and response characteristics of nitrifying functional genes in tannery sludge contaminated soil. Journal of Groundwater Science and Engineering, 10(3): 223−232. DOI：10.19637/j.cnki.2305-7068.2022.03.002.

Kumar A, Pramod Krishna A. 2020. Groundwater vulnerability and contamination risk assessment using GIS-based modified DRASTIC - LU model in hard rock aquifer system in India. Geocarto International, 35: 1149−1178. DOI：10.1080/10106049.2018.1557259.

Levin N, Kyba CCM, Zhang QL, et al. 2020. Remote sensing of night lights: A review and an outlook for the future. Remote Sensing of Environment, 237: 111443. DOI：10.1016/j.rse.2019.111443.

Liu YC, Fei YH, Li YS, et al. 2024. Pollution source identification methods and remediation technologies of groundwater: A review. China Geology, 7(1): 125−137. DOI：10.31035/cg2022080.

Lubianetzky TA, Dickson SE, Guo Y. 2015. Proposed method: incorporation of fractured rock in aquifer vulnerability assessments. Environmental Earth Sciences, 74: 4813−4825. DOI：10.1007/s12665-015-4471-y.

Ma L, Lu J, Zhao H, et al. 2018. Nitrate Vulnerable Zones and strategies of non-point pollution mitigation in China. Journal of Agro-Environment Science, 37: 2387−2391. DOI：10.11654/jaes.2018-1369.

Martínez-Bastida JJ, Arauzo M, Valladolid M. 2010. Intrinsic and specific vulnerability of groundwater in central Spain: the risk of nitrate pollution. Hydrogeology Journal, 18: 681−698. DOI：10.1007/s10040-009-0549-5.

Mekonnen MM, Hoekstra AY. 2016. Four billion people facing severe water scarcity. Science Advances, 2: e1500323. DOI：10.1126/sciadv.1500323.

Monteny GJ. 2001. The EU Nitrates Directive: A European approach to combat water pollution from agriculture. The Scientific World Journal, 1: 927−935. DOI：10.1100/tsw.2001.377.

Nahin KTK, Basak R, Alam R. 2020. Groundwater vulnerability assessment with DRASTIC index method in the salinity-affected southwest coastal region of Bangladesh: A case study in Bagerhat Sadar, Fakirhat and Rampal. Earth Systems and Environment, 4: 183−195. DOI：10.1007/s41748-019-00144-7.

Orellana-Macías JM, Merchán D, Causapé J. 2020. Evolution and assessment of a nitrate vulnerable zone over 20 years: Gallocanta groundwater body (Spain). Hydrogeology Journal, 28: 2207−2221. DOI：10.1007/s10040-020-02184-0.

Peng SZ, Ding YX, Liu WZ, et al. 2019. 1 km monthly temperature and precipitation dataset for China from 1901 to 2017. Earth System Science Data: 1931–1946. DOI:10.5194/essd-11-1931-2019

QMEEB (Quanzhou Municipal Ecological Environment Bureau). 2021. Water ecology of key river Basins in Quanzhou City during the 14th Five-Year Plan period Environmental protection planning. http://sthjj.quanzhou.gov.cn

Sidibe AM, Lin X. 2018. Heavy metals and nitrate to validate groundwater sensibility assessment based on DRASTIC models and GIS: Case of the upper Niger and the Bani basin in Mali. Journal of African Earth Sciences, 147: 199–210. DOI：10.1016/j.jafrearsci.2018.06.019.

Smail RQS, Dişli E. 2023. Assessment and validation of groundwater vulnerability to nitrate and TDS using based on a modified DRASTIC model: A case study in the Erbil Central Sub-Basin, Iraq. Environmental Monitoring Assessment, 195: 567. DOI：10.1007/s10661-023-11165-1.

Stigter TY, Ribeiro L, Dill AMMC. 2006. Evaluation of an intrinsic and a specific vulnerability assessment method in comparison with groundwater salinisation and nitrate contamination levels in two agricultural regions in the south of Portugal. Hydrogeology Journal, 14: 79–99. DOI：10.1007/s10040-004-0396-3.

Sun XB, Guo CL, Zhang J, et al. 2023. Spatial-temporal difference between nitrate in groundwater and nitrogen in soil based on geostatistical analysis. Journal of Groundwater Science and Engineering, 11: 37–46. DOI：10.26599/JGSE.2023.9280004.

Tao M, Lai S, Deng Y. 2002. 1: 250, 000 hydrogeologic map of the southern coastal area of Fujian.

Verma A, Sharma A, Kumar R, et al. 2023. Nitrate contamination in groundwater and associated health risk assessment for Indo-Gangetic Plain, India. Groundwater for Sustainable Development, 23: 100978. DOI:10.1016/j.gsd.2023.100978.

Xu XL, Liu JY, Zhang SW, et al. 2018. China's Multi-Period Land Use Land Cover Remote Sensing Monitoring Dataset (CNLUCC). DOI:10.12078/2018070201.

Yankey RK, Anornu GK, Osae SK, et al. 2021. Drastic model application to groundwater vulnerability elucidation for decision making: the case of south western coastal basin, Ghana. Modeling Earth Systems and Environment, 7: 2197–2213. DOI：10.1007/s40808-020-01031-1.

Zenebe GB, Hussien A, Girmay A, et al. 2020. Spatial analysis of groundwater vulnerability to contamination and human activity impact using a modified DRASTIC model in Elalla-Aynalem Catchment, Northern Ethiopia. Sustainable Water Resources Management, 6: 51. DOI：10.1007/s40899-020-00406-7.

Zhong ZX, 2005. A discussion of groundwater vulnerability assessment method. Earth Science Frontiers, 12: 3–013.